Dynamics of the 4-Day Wave in the Southern Hemisphere Polar Stratosphere

WILLIAM J. RANDEL

National Center for Atmospheric Research, Boulder, Colorado*

LESLIE R. LAIT

Universities Space Research Association, Laboratory for Atmospheres, NASA/Goddard Space Flight Center, Greenbelt, Maryland

(Manuscript received 20 June 1990, in final form 22 April 1991)

ABSTRACT

Dynamics of the 4-day wave in the Southern Hemisphere polar stratosphere is investigated using horizontal wind and temperature data. These were derived from synoptic maps of satellite-measured brightness temperatures, which were generated using the fast Fourier synoptic mapping technique of Salby. Circulation statistics from these data are compared to those from the National Meteorological Center (NMC) operational stratospheric analyses, demonstrating improvements afforded by detailed treatment of asynoptic sampling effects. The 4-day wave is isolated using temporally filtered data. Several events of wave growth and decay are observed in the upper stratosphere during August 1980. Derived zonal-mean and eddy statistics suggest that the 4-day wave results from an instability of the zonal-mean flow near 55°–60°S, at and above 1 mb. Inspection of climatological data suggests the source of the instability to be the "double-jet" structure in the upper stratosphere and mesosphere (the subtropical mesospheric jet near 30°S and the high-latitude extension of the polar night jet near 70°S). Contribution of the 4-day wave to the general circulation of the stratosphere is discussed: one feature attributable to the 4-day wave is a region of positive EP flux divergence in the upper stratosphere near 50°–60°S.

1. Introduction

The 4-day wave is an eastward-propagating planetary wave disturbance present in polar latitudes of the winter stratosphere. It was first observed in satellite radiance measurements by Venne and Stanford (1979), and further observations were reported in Venne and Stanford (1982) and Prata (1984). Lait and Stanford (1988) have recently applied the fast Fourier synoptic mapping technique of Salby (1982) to polar-orbiting satellite radiance data, yielding high-resolution space–time spectra and high quality synoptic maps of the 4-day wave. These studies have yielded the following characteristics of temperature fluctuations associated with the 4-day wave:

1) The 4-day wave is a winter hemisphere phenomenon, observed in both hemispheres. It is substantially stronger in the SH, and most analyses have focused there. Temperature power spectra show variance maxima confined to polar regions, centered near 60°–70° latitude. Venne and Stanford (1982) note a somewhat faster period in the SH (3.6 days) versus that in the NH (4.4 days).

2) The 4-day wave exhibits small vertical phase tilts with height in the stratosphere. Temperature variances increase with height below approximately 45 km. This vertical structure is termed equivalent barotropic. Prata (1984) is the only study to analyze data above the stratopause, noting small amplitudes at 62 and 85 km.

3) Eastward-propagating power is evident for zonal waves 1–4. Higher zonal-wavenumber components move with successively faster frequencies, such that all components travel with the same zonal phase velocity. Reconstructed synoptic maps reveal one or more "warm pools" circling the pole with period near 4 days (Prata 1984, his Fig. 5; Lait and Stanford 1988, their Figs. 7–10). These features are remarkably long lived; Lait and Stanford (1988) show that one such pool retains its identity for at least seven complete revolutions about the pole.

4) The horizontal phase structure is a variable based on the above studies. Because direction of the zonally averaged meridional momentum flux is most relevant dynamically (see section 3) and directly related to latitudinal phase tilt for plane waves, we discuss the latitudinal structure observed in these works in terms of the inferred momentum fluxes. Venne and Stanford (1979, 1982) find poleward fluxes in the NH and equatorward fluxes in the SH for the 4-day wave. Prata

* The National Center for Atmospheric Research is sponsored by the National Science Foundation.

Corresponding author address: William J. Randel, NCAR, P.O. Box 3000, Boulder, CO 80307-3000.

(1984) finds poleward fluxes in the SH for July 1973, but states that observations from other months tend to be quite variable.

Regarding the somewhat ambiguous results in (4), Manney (1991) has studied the zonal wave-1 component of the 4-day wave based on 10 years of National Meteorological Center (NMC) geopotential height data. She finds episodes of wave growth characterized by two distinct types of structure: one with poleward momentum fluxes in high latitudes and the other with equatorward fluxes. Manney proposes two distinct types of instability to underlie these observations.

This work is an observational study of the dynamics of the 4-day wave in the SH during one month studied by Lait and Stanford (1988). We use their high quality synoptically reconstructed brightness temperature data to generate temperatures, geopotential heights, and horizontal winds at several pressure levels in the middle and upper stratosphere. Temperature data and some derived fields are compared to those from operational NMC products for the same time period, revealing improvements afforded by the synoptic mapping technique. Time filtering is used to isolate characteristics of the 4-day wave. Several events of wave growth and decay are observed in the upper stratosphere during August 1980. Eddy statistics show equatorward momentum flux in polar latitudes with positive EP flux divergence near 55°–60°S, and the zonal-mean flow is found to be unstable in this latitude band at and above 1 mb. Furthermore, episodes of wave growth occur in tandem with or subsequent to periods of strongest zonal-mean instability. These observations suggest that the 4-day wave during this month results from an instability of the zonal-mean flow over 55°–60°S latitude at and above 1 mb. Inspection of climatological wind fields suggests this instability arises in the upper stratosphere and mesosphere, in a region sandwiched by the subtropical mesospheric jet and a high latitude extension of the polar night jet. The fundamental character of this instability is barotropic, consistent with the observed equivalent barotropic signature of the 4-day wave (signified by a predominance of wave momentum fluxes over heat fluxes). We do, however, find that one of the several events here has a significant baroclinic component (comparatively large heat fluxes); this suggests that baroclinic excitation near the stratopause may occasionally contribute to the 4-day wave. The effect of the 4-day wave on the general circulation of the stratosphere is discussed, and we note that one signature of the 4-day wave is a region of positive EP flux divergence in the upper stratosphere near 50°–60°S.

2. Data and analyses

a. *Calculation of temperature profiles and winds*

The data analyzed here are grids of temperature and horizontal winds generated from the synoptically mapped brightness temperature data that are presented in Lait and Stanford (1988), along with base-level geopotential data from the Climate Analysis Center of the National Meteorological Center (CAC/NMC). Brightness temperature data for August 1980 are available from three separate channels of the Stratospheric Sounding Unit on board *NOAA-6* (SSU1, SSU2, and SSU3). The weighting functions for these channels (see Smith et al. 1979, their Fig. 1) peak near 2, 5, and 15 mb and have a vertical half-width near 15 km. Vertical temperature profiles at pressure levels p_i were generated from these brightness temperature (TB) data via linear regression:

$$T(p_i) = W_{1i} \cdot \mathrm{TB}_{\mathrm{SSU1}} + W_{2i} \cdot \mathrm{TB}_{\mathrm{SSU2}} + W_{3i} \cdot \mathrm{TB}_{\mathrm{SSU3}}. \quad (1)$$

Pressure levels for the analyses were 30, 10, 5, 2, and 1 mb. This linear regression scheme is basically the same as that used to generate the temperature profiles archived operationally by CAC/NMC (see Smith et al. 1979). The regression coefficients (W_{1i}, W_{2i}, W_{3i}) used here were calculated by regressing gridded temperature profiles upon gridded SSU1, SSU2, and SSU3 brightness temperature data, both obtained from the standard operational CAC/NMC archive. These latter data were gridded using a standard successive correction (Cressman) analysis (Gelman and Nagatani 1977). The regression coefficients were obtained from data during August 1981, when the same instrument on *NOAA-6* was still in operational use. We used the August 1981 data to generate the regression coefficients because the archived CAC/NMC temperature profiles for August 1980 were derived using only channels SSU1 and SSU2 (Gelman et al. 1986). The overall goal is to generate temperature profiles from the SSU data in an identical manner to that used operationally, but using SSU data that have the increased space–time resolution afforded by the fast Fourier synoptic mapping. Regression coefficients were generated for 10° latitude bins with data sampled every 30° longitude, over 20 days of once-daily data. The Cressman-analyzed grids were first smoothed horizontally by truncation at zonal wavenumber 4 to remove small-scale features. For the pressure levels analyzed, greater than 95% of the temperature profile variance (in time) was linearly related to the brightness temperature data.

Geopotential height thicknesses (ΔZ_i) for the layer p_i to p_{i+1} were calculated hydrostatically from the temperature profiles according to

$$\Delta Z_i = \frac{R}{g} \ln\left(\frac{p_i}{p_{i+1}}\right) \cdot \left[\frac{T(p_i) + T(p_{i+1})}{2}\right], \quad (2)$$

with $R/g = 29.29$ m K^{-1}. The quantity in brackets represents the mean temperature for the layer p_i to p_{i+1}. These geopotential thicknesses are added to base-level geopotential data at 50 mb, obtained from the CAC/NMC archive. The synoptically mapped brightness temperatures (and resultant temperature grids)

are available twice daily; base-level heights are once-daily 1200 UTC analyses, and we simply interpolate to twice-daily data. As discussed in Lait and Stanford (1988), a second set of brightness temperature grids were constructed by digitally filtering the temperature data to retain only the 4-day wave (the filter is shown in their Fig. 9). To be consistent with this treatment, the twice-daily base-level heights were also filtered to retain only the zonal mean and eastward-moving zonal waves 1–4 with periods shorter than 5 days. These data are referred to below as "filtered."

Horizontal winds were calculated from the geopotential data by linearization of the momentum equations about the zonal mean flow, which is in turn calculated using gradient wind balance (Randel 1987). The data here are all available on a 3° latitude grid, and zonal Fourier coefficients up to zonal wave 6 are retained (only up to wave 4 for the filtered data, because higher wavenumbers are beyond the Nyquist limit—see Lait and Stanford 1988).

Lait and Stanford (1988) presented analyses for three months of data: June 1979, August 1979, and August 1980. The 4-day wave was present only during June 1979 and August 1980. Data for June 1979 have the disadvantage that only the two lower channels (SSU1 and SSU2) were operational. We thus focus this study on dynamics of the 4-day wave during August 1980.

b. *Comparisons with CAC/NMC operational analyses*

In this section we make some comparisons between our data and CAC/NMC operational analyses covering the same time period. The fundamental difference between these data is the horizontal mapping used: our data are based on the fast Fourier synoptic (FFS) mapping discussed in detail in Lait and Stanford (1988), while the CAC/NMC (hereafter NMC) data are produced via the Cressman scheme. Direct comparison between the two illustrate advantages of the FFS mapping, in particular in a region where much of the variance is on a fast time scale. A limitation of this comparison is that the NMC temperature and geopotential data for this time period are based on SSU1 and SSU2 brightness temperatures only, and NMC data at 2 and 1 mb are mainly extrapolation from below. We thus focus our comparisons on the 5-mb level.

Figure 1 shows horizontal maps of the 5-mb temperature for 1200 UTC 26 August from the two datasets, with the zonal means removed to accentuate the wave components (zonal means are not affected by the mapping schemes). The 4-day wave is associated with the two "warm pools" near 60°S, 90°E and 150°W seen in both data; see Lait and Stanford (1988) for a sequence of similar maps showing the wave propagation. The comparison in Fig. 1 shows overall similar patterns for the FFS and NMC data, but there is a significant gain in detail afforded in the FFS analyses. Although the NMC grids approximately capture the maximum and minimum near 90°E and 90°W, other extrema are underestimated by up to 6 K in the NMC analyses.

Figure 2 shows latitude–time sections of the zonal wave 1–6 temperature variance at 5 mb from the FFS and NMC data. Variance based on the Cressman scheme is typically about half that found using the FFS analyses, consistent with the comparisons shown in Fig. 1. Figure 3 shows similar diagrams for a more highly derived quantity, the zonally averaged momentum flux. Similar overall patterns are found in the two data in Fig. 3, although the NMC grids underestimate some local maxima by ~30%–50%. The NMC grids also omit the maximum near 40°–50°S over 26–27 August.

Figure 4 shows EP flux diagrams for FFS and NMC data averaged over the entire month of August. As discussed above, differences below ~40 km are mainly due to the different horizontal mappings used; above this level, the additional information in SSU3 is included in the FFS data. One effect of this additional information is an increase in the baroclinic wave structure at 1 mb in the FFS data (larger vertical components of the EP flux vectors). Both sections in Fig. 4 show positive divergence over 50°–60°S, with negative values at higher and lower latitudes. Divergences evaluated with the FSS data are stronger than those from the NMC data, mainly due to the increased FFS momentum fluxes (Fig. 3).

3. Signatures of barotropic instabilities

In section 4 we examine the zonal-mean flow and eddy statistics to determine the source mechanism for the 4-day wave during August 1980. These results are interpreted in light of the necessary conditions for mean flow instability, along with the eddy signatures anticipated for an instability. At the level of quasigeostrophic theory, the necessary condition for a zonal wind ($\bar{u}$) structure to be unstable is that the meridional gradient of potential vorticity ($\bar{q}_y$) become negative:

$$\bar{q}_y \equiv \beta - \bar{u}_{yy} - \rho_0^{-1}\left(\rho_0 \frac{f^2}{N^2}\bar{u}_z\right)_z < 0, \qquad (3)$$

(e.g., Andrews et al. 1987). One signature expected of an instability is growth of wave activity in tandem with or subsequent to appearance of $\bar{q}_y < 0$, and below we show such behavior. As a note, although the second term in (3) is written as $\bar{u}_{yy}$, calculations using the full spherical terms are used. Also, we include the full latitude–height dependence of f^2/N^2 in (3) and smooth the resulting $\bar{q}_y$ field 1–2–1 in latitude.

The observed in-phase vertical structure of the 4-day wave suggests its dynamics are fundamentally barotropic in nature. Prompted by this observation, Hartmann (1983) originally proposed barotropic instability of the polar night jet stream as an excitation mechanism for the 4-day wave. Hartmann found fast

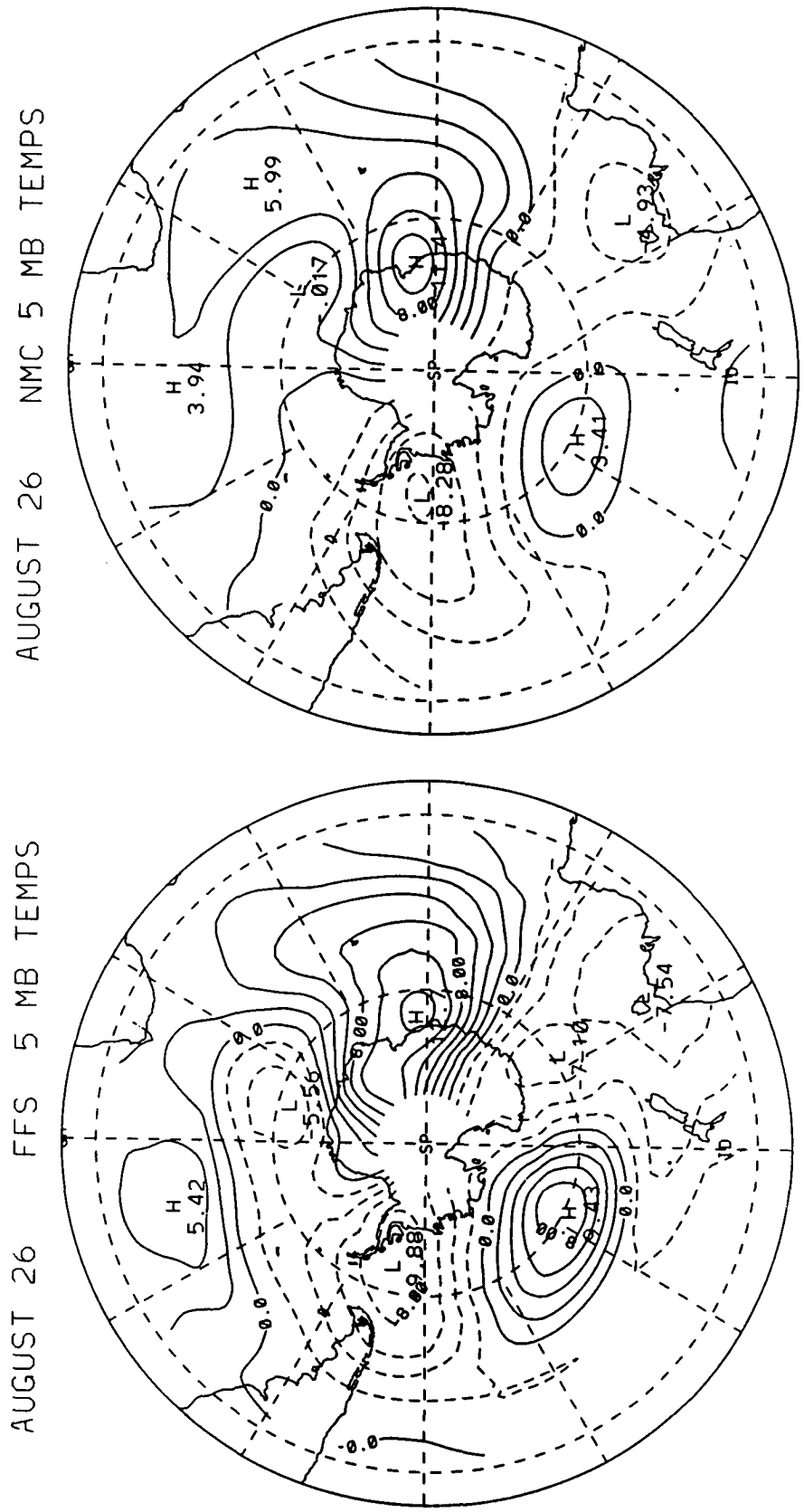

FIG. 1. Polar stereographic maps of the 5-mb temperature on 26 August 1980, derived from satellite data mapped using FFS (left) and NMC Cressman (right) analyses. Zonal means have been removed to accentuate the wave components. Contour interval is 2 K.

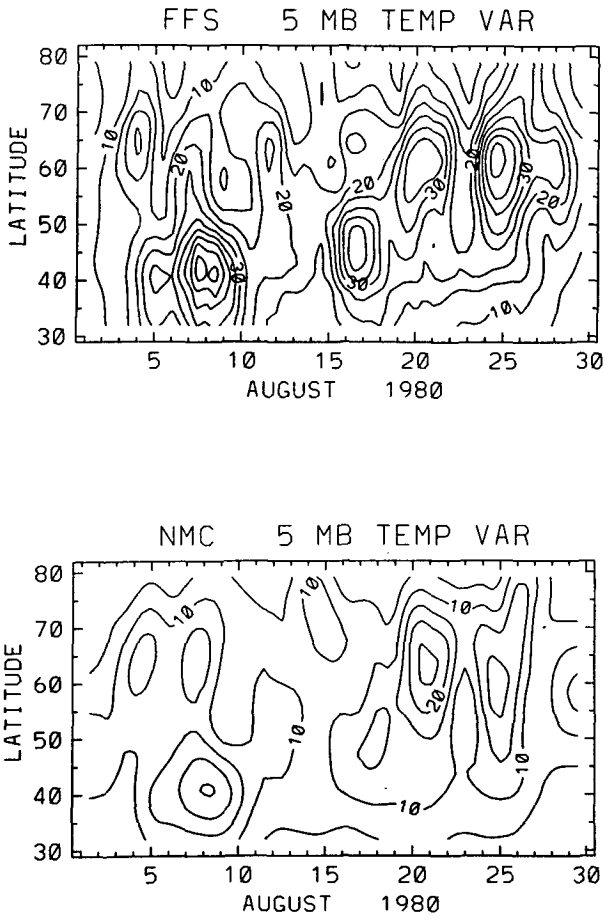

FIG. 2. Latitude–time sections over August 1980 of the 5-mb temperature variance for zonal waves 1–6, from FFS (top) and NMC Cressman analyses (bottom). Contour interval is 5 K^2. In these and the following figures, the latitude axis refers to latitude south.

eastward-traveling polar modes resulting from unstable shears (and associated $\bar{q}_y < 0$) on the poleward flank of idealized stratospheric jets. Manney et al. (1988) confirmed these results using observed stratospheric winds. The fundamental signature of such unstable modes is *poleward* momentum flux in high latitudes, with a dipole pattern of EP flux divergence (positive to the poleward side), which acts to decelerate the jet core and accelerate the poleward flank (see Hartmann, his Fig. 12). The wave thus acts to remove the unstable shears in the wind profile; this is a general result for linear instabilities, which is of utility for assessing the unstable wind profile at their source.

A second type of barotropic instability, which may be of relevance here, is that of a double-jet structure, with the central minimum a region of negative vorticity gradient. An idealized situation of this type was analyzed by Schoeberl and Lindzen (1984), in the context of a point jet instability. The fundamental signature of this mode is *equatorward* momentum flux on the poleward side of the unstable region, and poleward flux on the equatorward side (see Schoeberl and Lindzen, their Fig. 6). The resulting EP flux divergence is positive in the central $\bar{q}_y < 0$ region and negative to the sides, again acting to remove the unstable flow profile. These two contrasting types of instability and their resulting signatures in the momentum flux fields are analyzed and discussed further in Manney (see her Figs. 9 and 11). A general result obtained from these linear instability studies is that the EP flux divergence is positive near the region $\bar{q}_y < 0$ that is the source of the instability [as noted in Hartmann 1983, his Eq. (7)]. This result is applied to the observed EP flux signatures here to locate the underlying unstable region.

4. Results—The 4-day wave during August 1980

The August average structure of the zonal-mean fields $\bar{u}$ and $\bar{q}_y$ are shown in Fig. 5. The polar night jet maximizes over 80 m s^{-1} near 35 km, 50°–60°S. The base of the subtropical mesospheric jet is seen at 1 mb over 40°–50°S. A region of weak $\bar{q}_y$ is found in the minimum region between these jets, extending to both

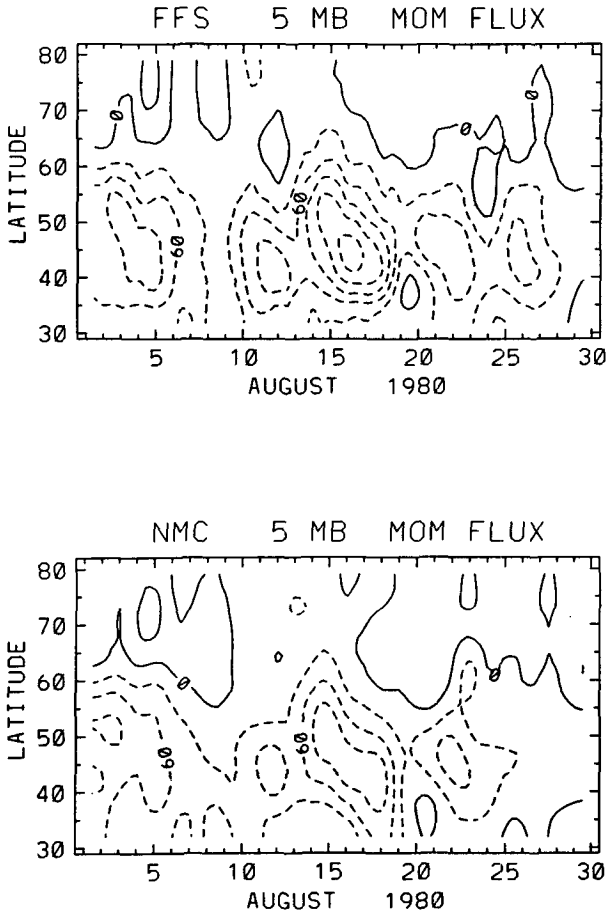

FIG. 3. Latitude–time sections over August 1980 of the 5-mb meridional momentum flux for zonal waves 1–6, from FFS (top) and NMC Cressman analyses (bottom). Contour interval is 30 m^2 s^{-2}.

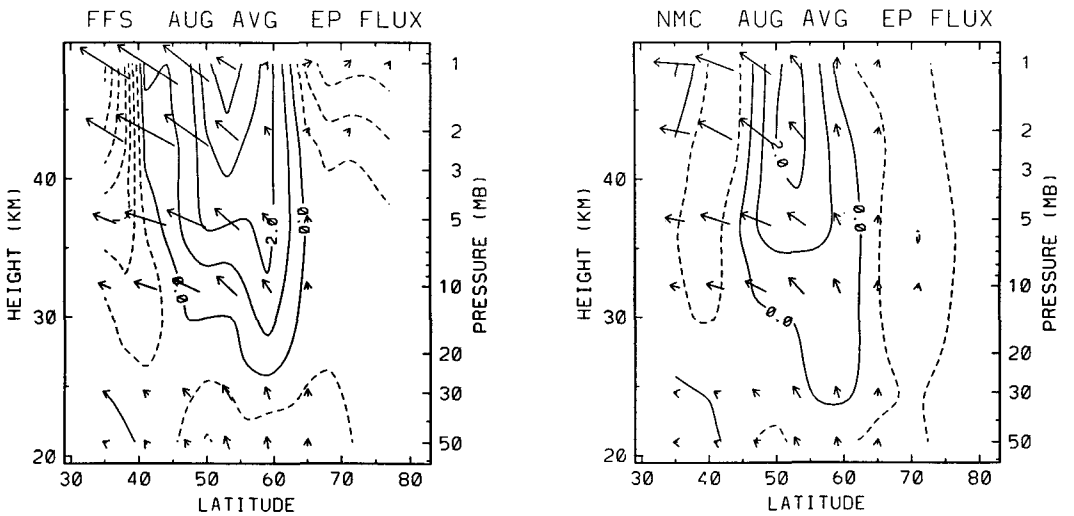

FIG. 4. August 1980 average EP flux diagrams derived from FFS (left) and NMC Cressman analyses (right). Contour interval is 1 m s^{-1}/day.

flanks of the jet at 1 mb. Latitudes poleward of 72°S also show $\bar{q}_y < 0$ throughout the stratosphere.

Time evolution of the 1-mb $\bar{u}$ and $\bar{q}_y$ fields are shown in Fig. 6. There is a zonal wind maximum over 40°–50°S throughout the month, with a weak secondary maximum near 65°S after 22 August. The $\bar{q}_y$ field shows maxima near 40° and 65°S sandwiching a minimum region over 55°–60°S, along with high- and low-latitude $\bar{q}_y < 0$ areas. The 55°–60°S band shows several time periods where $\bar{q}_y < 0$, as highlighted in Fig. 6b.

Dynamical signatures of the 4-day wave at 1 mb are shown in the series of latitude–time diagrams in Fig. 7, all calculated from filtered data. Temperature variance (Fig. 7a) shows growth and decay of wave activity for several apparently individual events. Note that the brightness temperature spectral signatures in Lait and Stanford (1988), calculated for the entire month of August, are effectively averages over these individual events. The momentum flux patterns (Fig. 7b) also show this episodic nature with two pronounced maxima (9–13 and 23–27 August) and a smaller maximum for 16–18 August (as indicated in Fig. 7b). The patterns are somewhat different between events: 9–13 August shows a dipole pattern of fluxes centered near 50° and 65°S (directed toward their center), while 23–27 August has a single equatorward maximum centered near 60°–70°S. The strong equatorward flux throughout the month poleward of 60°S is a robust signature of the

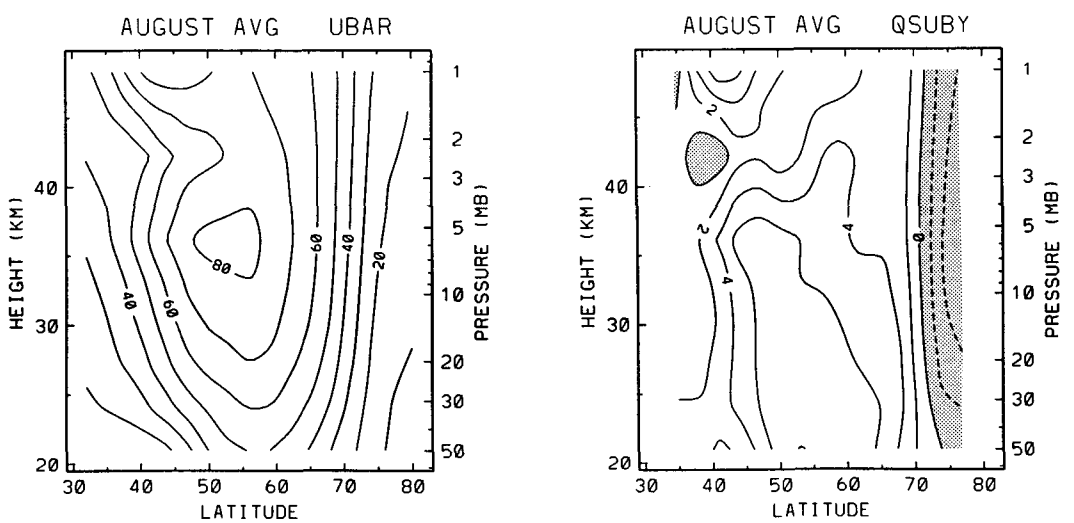

FIG. 5. August average zonal-mean zonal wind (m s^{-1}) and quasigeostrophic potential-vorticity gradient (10^{-11} m^{-1} s^{-1}).

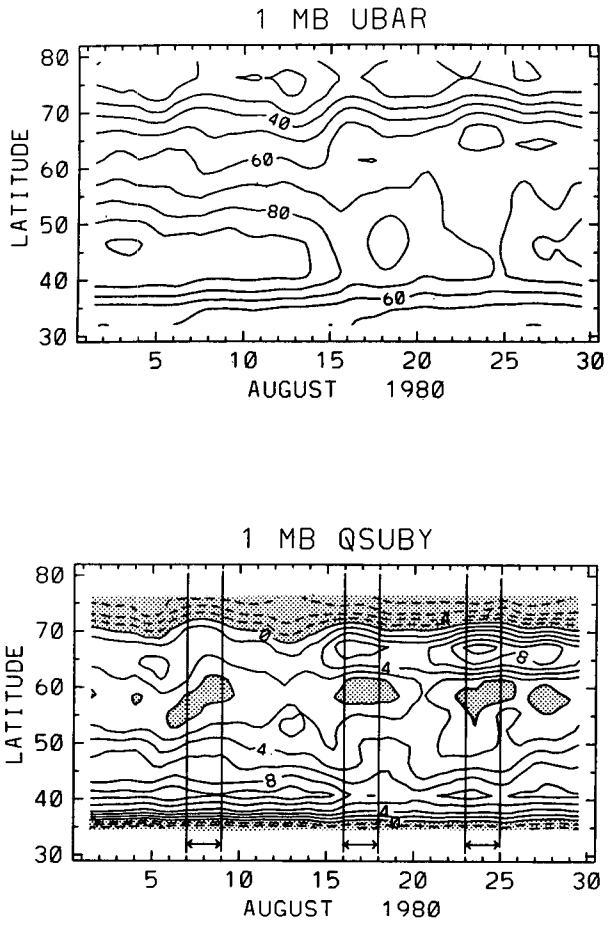

FIG. 6. Latitude–time sections of the 1-mb zonal wind (top) and quasigeostrophic potential-vorticity gradient (bottom). Contours as in Fig. 5. Arrows in the lower panel highlight times when $\bar{q}_y < 0$ over 55°–60°S.

4-day wave and is the first evidence that a poleward flank instability of the polar night jet is not the source mechanism (see discussion in section 3).

Zonally averaged heat fluxes for the 4-day wave at 1 mb (Fig. 7c) are evident only for the event of 23–27 August, with a sign indicating equatorward flux. Although in the monthly average the heat fluxes are small (consistent with the in-phase vertical structure found in statistical studies of the 4-day wave), for this one event they are significant (as discussed further).

Figure 7d shows the EP flux divergence attributable to the 4-day wave. The patterns show a dipole pattern of positive values over 50°–60°S and negative values poleward of 65°S throughout the month, with maximum values for the individual events noted above. An important feature to note is that the separate maxima in 4-day wave variance quantities, in particular the momentum flux and EP flux divergence (Figs. 7b–d), occur in tandem with or subsequent to the time periods where $\bar{q}_y < 0$ over 55°–60°S in Fig. 6b. This is the behavior expected if the 4-day wave arises from an instability associated with the latter region (in contrast, similar coherent behavior is not observed for the high- and low-latitude $\bar{q}_y < 0$ regions in Fig. 6b).

The relative importance of wave fluxes by the 4-day wave at 1 mb can be assessed by comparison with fluxes from the total (unfiltered) data shown in Figs. 8a,b. Comparison of the momentum fluxes (Figs. 7b and 8a) shows that the 4-day wave is responsible for almost all the equatorward flux observed poleward of 60°S, whereas it contributes little of the poleward flux in lower latitudes (especially away from 9 to 13 August). The 4-day wave EP flux-divergence dipole patterns observed during the three events (Fig. 7d) are seen in the total field (Fig. 8b), although there is much additional variability from the other wave components. Figure 8c shows the observed $\partial\bar{u}/\partial t$ at 1 mb. There is reasonable agreement with the total wave-driving patterns in Fig. 8b, with temporal correlations varying with latitude from 0.3–0.7. North–south dipole patterns observed of the 4-day wave driving (Fig. 7d) are observed in $\partial\bar{u}/\partial t$, most clearly for the events of 16–18 and 23–28 August.

Stability calculations for planetary waves typically give results for individual zonal wave numbers (e.g., Hartmann 1983 and Manney et al. 1988), and for comparison it is of interest to study wave characteristics for individual components of the 4-day wave. Lait and Stanford demonstrated statistically that the 4-day wave during August 1980 had components from zonal waves 1–4 (their Fig. 2). We find wave 4 to contribute insignificantly to the variance quantities and show in Fig. 9 temperature variances and momentum fluxes for zonal waves 1–3. Wave maxima during 9–13 August are contributed by waves 2–3; although both show equatorward fluxes poleward of 60°S, only wave 3 exhibits the poleward fluxes in lower latitudes seen in the 4-day total (Fig. 7b). The 23–28 August event has the largest temperature variance for wave 2, although waves 1–3 contribute to the high-latitude equatorward momentum fluxes. The 16–18 August event has relatively large wave 1 temperature variance but almost no momentum flux at 1 mb, while fluxes from waves 2–3 cancel to a large degree near 55°S. There is an additional wave 1 event over 2–4 August not discussed previously. Both this and the wave-1 component over 23–28 August exhibit a double-peaked temperature variance pattern (maxima near 55° and poleward of 70°S) and equatorward fluxes over 60°–80°S. Wave 1 also shows a polar variance maximum for 13–15 August with weak poleward flux. Overall, the wave signatures evolve strongly over the month, and statistical signatures (time averages or spectral analyses) will show a washed-out version of the instantaneous wave structures.

The structure of the mean flow and average EP flux signature of the 4-day wave for the event of 9–13 August are shown in Fig. 10. The zonal-mean structure

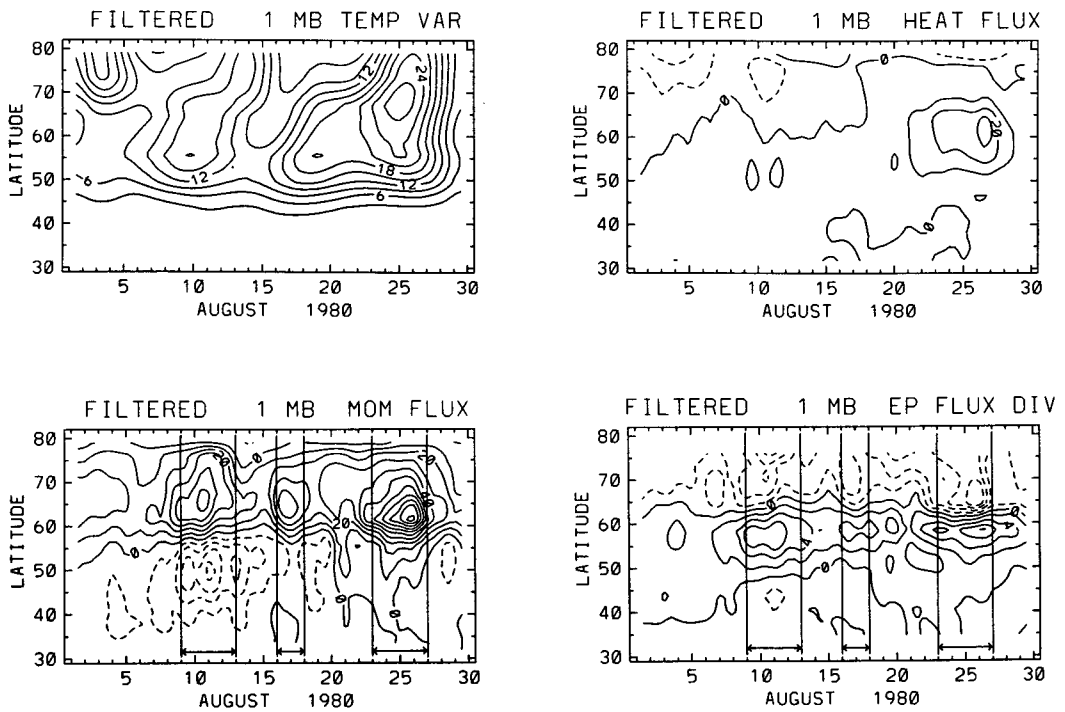

FIG. 7. Latitude–time sections at 1 mb of 4-day-wave quadratic quantities, calculated from filtered data. (a) Temperature variance (contours are 3 K^2), (b) meridional momentum flux (10 $m^2 s^{-2}$), (c) meridional heat flux (10 K m s^{-1}), and (d) EP flux divergence (2 m s^{-1}/day). Arrows in the lower panels denote episodes of maximum 4-day-wave activity.

looks much like the August average (Fig. 5), with a slightly stronger jet at 1 mb, and additional areas of $\bar{q}_y < 0$ near 2 mb, 52°S and above 1 mb at 60°S. The EP flux signature shows a predominant barotropic character, with horizontal divergence away from 55°–60°S. From the criterion that the positive EP flux divergence locates the unstable region (section 3), Fig. 10 suggests the poleward flank of the mesospheric jet, above 1 mb near 60°S, to be the source of the 4-day wave.

Figure 11 shows a climatological August zonal wind structure taken from Fleming et al. (1988). There is a pronounced region of $\bar{q}_y < 0$ above the stratopause over 40°–60°S, due to the double-jet structure found in the mesosphere (the subtropical mesospheric jet near 30°S and an upward extension of the polar night jet near 70°S). It is reasonable to postulate a similar unstable structure above 1 mb near 60°S during August 1980, of which only the base is seen in Fig. 10a.

Figure 12 shows time average zonal mean and 4-day wave EP signature for the 23–27 August event. The zonal-mean wind (Fig. 12a) shows a weaker jet at 1 mb, 40°–50°S than Fig. 10a, but stronger winds near 65° (see also Fig. 6a). This 1-mb structure hints at the double-jet structure seen in the mesosphere in Fig. 11, and there is a corresponding region of $\bar{q}_y < 0$ near 60°S in Fig. 12. The EP flux signature for this event shows a mixed baroclinic–barotropic character, with downward–poleward-pointing vectors and positive divergence near 60°S. This structure is even more suggestive of an instability in the mesosphere near 60°S. The downward-pointing EP flux vectors in Fig. 12 suggest a downward propagation of wave activity in the upper stratosphere.

A vertical section of the 4-day wave temperature variance at 65°S is shown in Fig. 13, and the two time periods studied in Figs. 10–12 are clearly emphasized. The 9–13 August event shows variance maxima occurring simultaneously at levels in the upper and middle stratosphere. The latter event shows maxima at 1–2 mb preceding those at lower altitudes (5–10 mb) by approximately one day, consistent with the downward propagation suggested in Fig. 12. In light of the highly derived nature of the EP flux quantities, and their associated uncertainty, it is encouraging to find consistent signatures in a more fundamental variable, such as temperature variance.

5. Discussion

a. Comparison of FFS and NMC mapped data

The results shown in Figs. 1–4 allow direct comparison of stratospheric circulation statistics derived

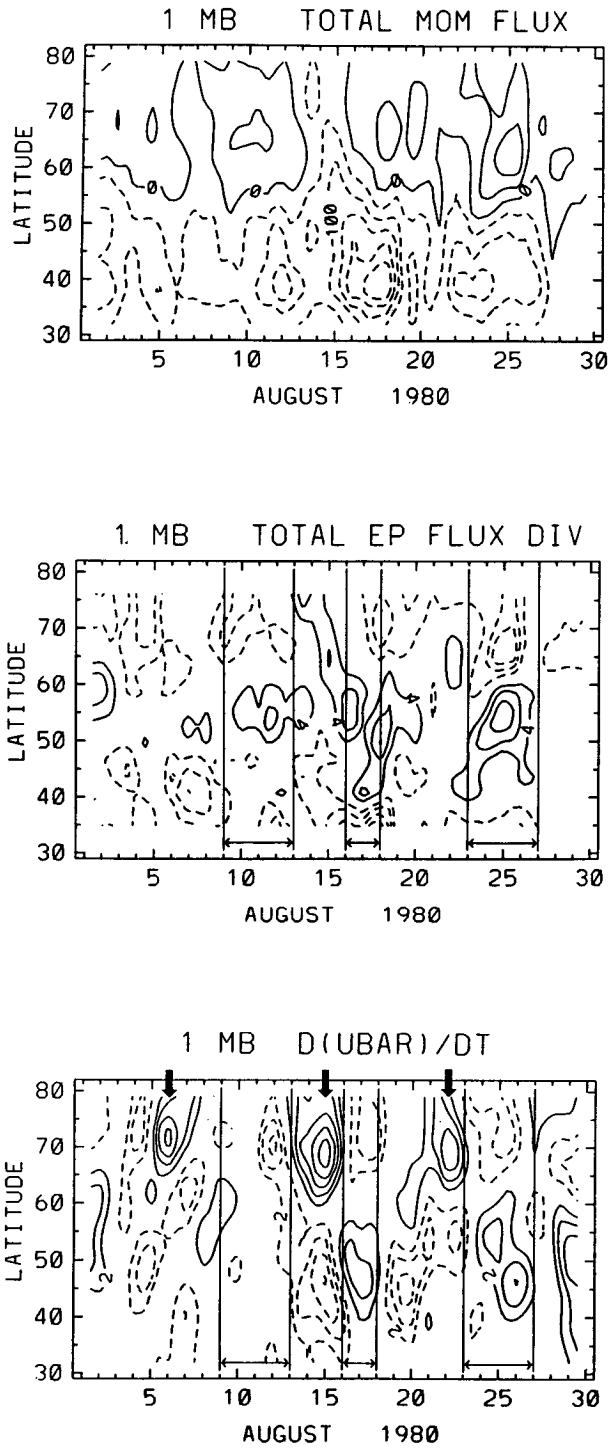

FIG. 8. Latitude–time sections at 1 mb of (a) meridional momentum flux (contours are 50 $m^2 s^{-2}$) and (b) EP flux divergence (4 m s^{-1}/day, zero contours omitted) for the total (unfiltered) data. Observed zonal-wind acceleration at 1 mb is shown in (c); contours are 2 m s^{-1}/day and zero contours are omitted. 4-day-wave event time periods highlighted in Fig. 7 are also noted in (b) and (c). Arrows above panel (c) point to zonal accelerations that occur just prior to the 4-day-wave events.

from polar-orbiting satellite data using the fast Fourier synoptic mapping procedure of Salby (1982) versus the successive correction (Cressman) analyses applied operationally at CAC/NMC. The FFS data show more detailed structure and increased wave variances, a result that is not surprising in a region where much of the variability is due to the 4-day wave. Momentum fluxes over 35°–55°S, which are mainly due to slower planetary waves, can be underestimated by ~30%–50% by the NMC data, although the overall space–time patterns are accurately captured. Climatologies based on NMC data may thus underestimate some of these derived quantities. In fairness, the FFS scheme involves a great deal more intensive data handling, in particular regarding the treatment of missing data, and is probably not suitable for operational requirements.

b. *Observed dynamics of the 4-day wave*

The fundamental signature of the 4-day wave shown here is that of equatorward momentum flux in high latitudes, and resulting positive EP flux divergence centered near 55°–60°S in the upper stratosphere. The zonal-mean flow exhibits $\bar{q}_y < 0$ in this latitude band at (and presumably above) 1 mb. Furthermore, growth in 4-day wave activity occurs in several events in tandem with or subsequent to appearance of $\bar{q}_y < 0$ in this region. These signatures are unmistakeable evidence that the 4-day wave during August 1980 results from an instability of the zonal-mean flow in this region. Note that the effect of the 4-day wave fluxes (as denoted in the EP flux divergence patterns) is to accelerate winds over 55°–60°S and decelerate winds poleward of 65°S, an effect which is actually found in the observed accelerations in Fig. 8c, thereby tending to remove the unstable wind profile (with the result that $\bar{q}_y$ becomes positive following the wave event—see Fig. 6b).

The good temporal correlation between growth of the 4-day wave and episodes of $\bar{q}_y < 0$ over 55°–60°S at 1 mb is strong evidence that the waves grow in response to the mean-flow instability. What causes the episodic mean flow changes that result in these $\bar{q}_y < 0$ regions? Inspection of Fig. 8c shows that, just prior to the $\bar{q}_y < 0$ and 4-day wave events, the 1-mb zonal winds exhibit strong accelerations near 70°S and decelerations equatorward of 60°S (these times are noted with arrows above Fig. 8c). These accelerations result in increased meridional wind shears, leading to the unstable conditions $\bar{q}_y < 0$ (compare Figs. 6 and 8c). These episodic mean flow changes are probably partly due to planetary wave events (distinct from the 4-day wave); note there are temporal maxima in the 40°–50° momentum fluxes at 5 and 1 mb (Figs. 3 and 8a) near these times. However, the observed EP flux patterns (Fig. 8b; cross sections not shown here) are not easily reconciled with the observed $\partial\bar{u}/\partial t$ patterns; in particular, the observed polar accelerations are larger than the EP flux diver-

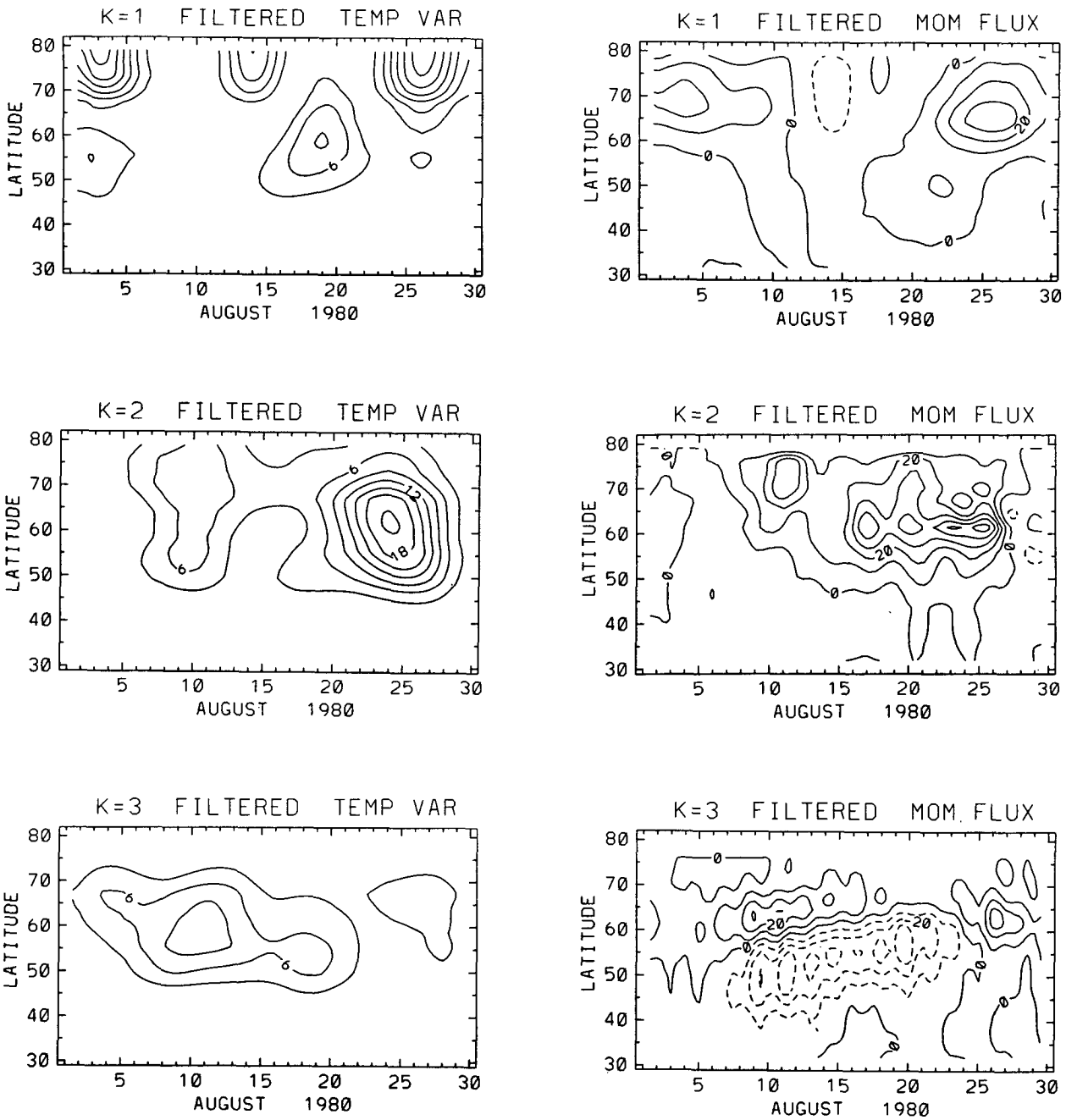

FIG. 9. Latitude–time sections at 1 mb of 4-day-wave temperature variances (left contours are 3 K^2) and meridional momentum fluxes (right, 10 $m^2 s^{-2}$) for individual zonal waves 1 (top), 2 (middle), and 3 (bottom).

gence anywhere in the stratosphere. This may suggest that other forcings (such as gravity-wave–driven circulations) may also contribute to these episodic accelerations.

Two of the 4-day-wave events exhibit a predominantly barotropic character (near absence of heat fluxes for 9–13 and 16–18 August), suggesting the instability is fundamentally barotropic in character. Poleward momentum fluxes are also found on the equatorward side of the unstable region at these times, and overall, the patterns are very similar to those found for the linear point jet instability of Schoeberl and Lindzen (1984). In contrast, the 23–28 August event exhibits a mixed barotropic–baroclinic signature. This mixed

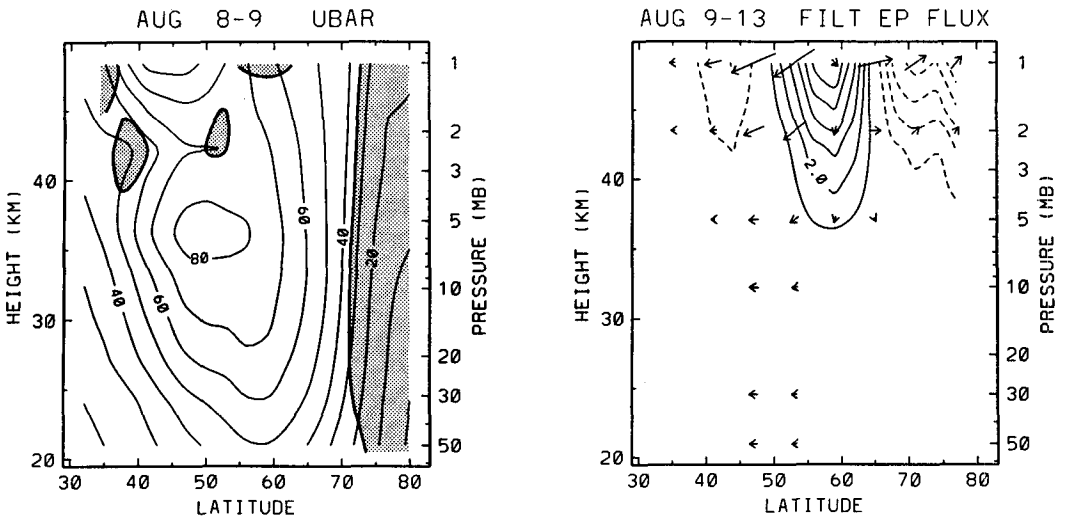

FIG. 10. (left) Zonal-mean zonal wind for 8–9 August. Heavy contours with shading denote $\bar{q}_y < 0$. (right) EP flux diagram for the 4-day wave (filtered data) averaged over 9–13 August. Contours are 1 m s^{-1}/day, and zero contours are omitted.

signature of the wave suggests the instability is partly baroclinic for this event. The nature of the baroclinic component is such that heat is transported toward the equator in the upper stratosphere, which is downgradient to the background of the warm polar stratopause. This association suggests that part of the excitation of the 4-day wave could be due to baroclinic instability at the stratopause.

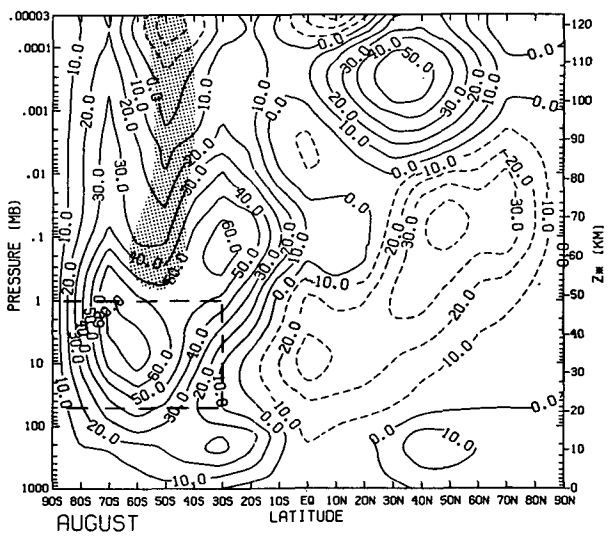

FIG. 11. Meridional cross section of zonal-mean winds (m s^{-1}) in August, taken from the climatology of Fleming et al. (1988). Shaded region in the SH denotes area where the quasigeostrophic potential-vorticity gradient is negative (also taken from Fleming et al. 1988). The boxed region denotes the area analyzed with the data in this study.

Inspection of climatological data (Fig. 11) shows a region of strong $\bar{q}_y < 0$ near and above 1 mb over the latitude band 40°–60°S. This unstable region lies between two jets in the mesosphere: the subtropical mesospheric jet near 30°S and an upward extension of the polar night jet near 70°S. In the mesosphere the unstable region is fundamentally barotropic in nature [due to the $\bar{u}_{yy}$ term in Eq. (3)]; the baroclinic ($\bar{u}_z$) term also tends toward instability near the stratopause. Much of the overall structure in this region is ultimately related to the very warm polar stratopause observed in SH winter, as recently discussed by Kanzawa (1989) and Hitchman et al. (1989). Hitchman et al. (1989) propose that the warm stratopause is due to gravity-wave–induced mean meridional motions, and the 4-day wave may be an example of planetary waves that are ultimately due to gravity waves.

The results of Manney (1991) support the hypothesis that two distinct types of instability are manifested as 4-day waves in the stratosphere (the 4-day period is probably due to advection by the mean winds and is similar for both cases—slower frequencies in the NH result from the observed weaker winds). A polar night jet instability results in high-latitude poleward momentum fluxes and likely corresponds to the observations for NH data analyzed by Venne and Stanford (1979, 1982) and the SH data in Prata (1984). The data shown here suggest an instability of the double-jet structure in the upper stratosphere and mesosphere, as signified by high-latitude equatorward momentum fluxes. The lack of a 4-day wave above the stratopause noted by Prata (1984) during June 1973, together with the observed poleward momentum fluxes, is consistent with a polar night jet instability during that time period.

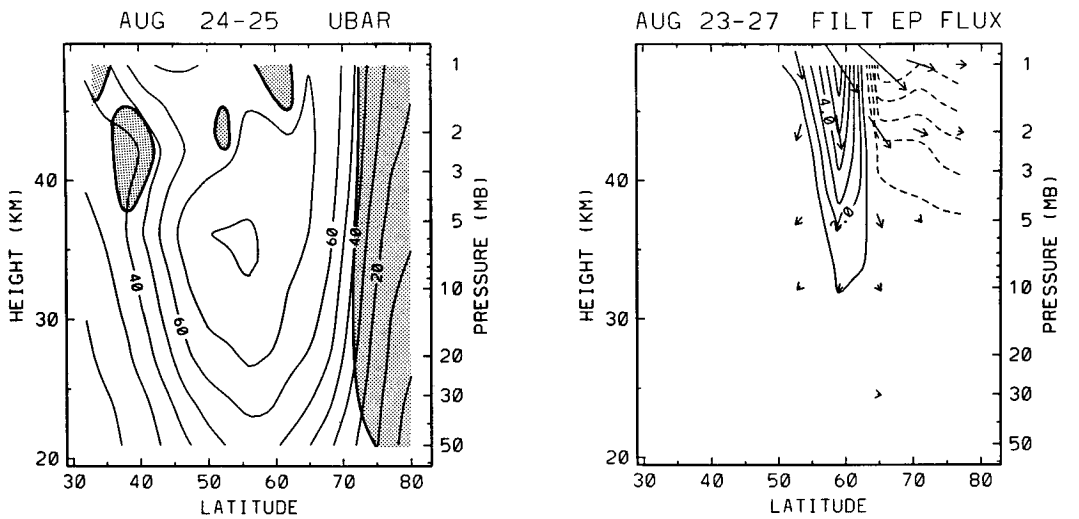

FIG. 12. (left) Zonal-mean zonal wind for 24–25 August. Heavy contours with shading denote $\bar{q}_y < 0$. (right) EP flux diagram for the 4-day wave (filtered data) averaged over 23–27 August. Contours are 1 m s^{-1}/day, and zero contours are omitted.

c. *General circulation influence of the 4-day wave*

The positive EP flux-divergence pattern observed of the 4-day wave over 50°–60°S in the upper stratosphere deserves some further comment. This feature is clearly seen in the unfiltered monthly average EP signature in Fig. 4; most of the positive values are due to the 4-day wave (cf. Figs. 7d and 8b). Positive EP flux divergences have been reported in the high-latitude winter stratosphere in climatological studies based on NMC data (Geller et al. 1983; Hartmann et al. 1984; Mechoso et al. 1985) and have been the subject of some discussion (Andrews 1987). Much if not all of the positive values in the *middle stratosphere* disappear when calculations are made using higher-order balanced (rather than geostrophic) winds (Randel 1987). However, strong positive values (of order 2 m s^{-1}/day) are present over 50°–60°S in the SH upper stratosphere for several different wind calculations (Randel 1987, his Fig. 25), suggesting they are a robust result. The results here, together with evidence for the regular presence of the 4-day wave in NMC data (Manney 1991), suggest that a sizeable fraction of those climatological patterns result from the 4-day wave.

Acknowledgments. We thank Rolando Garcia, Gloria Manney, and Kevin Trenberth for discussions and reviews of the manuscript. Constructive comments from two anonymous reviewers led to substantial revision and improvement of this paper. Marilena Stone expertly prepared the manuscript. WJR has been supported under NASA Grant W-16215.

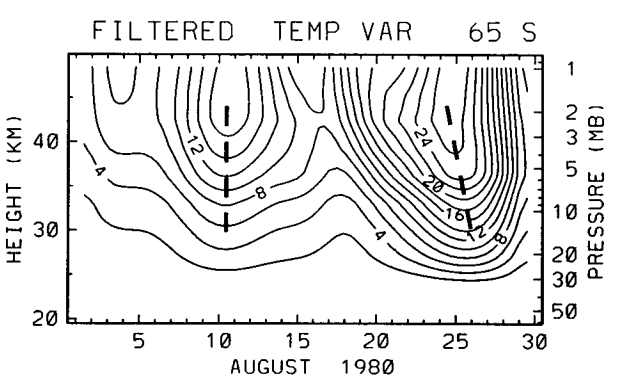

FIG. 13. Height–time section at 65°S of 4-day-wave temperature variance, calculated from filtered data. Contours are 2 K^2. Heavy dashed lines denote local maxima in time.

REFERENCES

Andrews, D. G., 1987: On the interpretation of the Eliassen–Palm flux divergence. *Quart. J. Roy. Meteor. Soc.*, **113**, 323–338.

——, J. R. Holton, and C. B. Leovy, 1987: *Middle Atmosphere Dynamics.* Academic Press, 489 pp.

Fleming, E. L., S. Chandra, M. R. Schoeberl, and J. J. Barnett, 1988: Monthly mean global climatology of temperature, wind, geopotential height and pressure for 0–120 km. NASA Tech. Memor. 100697, 85 pp.

Geller, M. A., M.-F. Wu, and M. E. Gelman, 1983: Troposphere-stratosphere (surface-55 km) monthly winter general circulation statistics for the Northern Hemisphere—four year averages. *J. Atmos. Sci.*, **40**, 1334–1352.

Gelman, M. E., and R. M. Nagatani, 1977: Objective analyses of height and temperature at the 5-, 2-, and 0.4-mb levels using meteorological rocketsonde and satellite radiation data. *COSPAR Space Res.*, **17**, 117–122.

——, A. J. Miller, K. W. Johnson, and R. M. Nagatani, 1986: Detection of long-term trends in global stratosphere temperature

from NMC analyses derived from NDAA satellite data. *Adv. Space Res.*, **6**, 17–26.

Hartmann, D. L., 1983: Barotropic instability of the polar night jet stream. *J. Atmos. Sci.*, **40**, 817–835.

——, C. R. Mechoso, and K. Yamazaki, 1984: Observations of wave-mean flow interactions in the Southern Hemisphere. *J. Atmos. Sci.*, **41**, 351–362.

Hitchman, M. H., J. C. Gille, C. D. Rodgers, and G. Brasseur, 1989: The separated polar winter stratopause: A gravity wave driven climatological feature. *J. Atmos. Sci.*, **46**, 410–422.

Kanzawa, H., 1989: Warm stratopause in the Antarctic winter. *J. Atmos. Sci.*, **46**, 435–438.

Lait, L. R., and J. L. Stanford, 1988: Fast, long-lived features in the polar stratosphere. *J. Atmos. Sci.*, **45**, 3800–3809.

Manney, G. L., 1991: The stratospheric 4-day wave in NMC data. *J. Atmos. Sci.*, **48**, 1798–1811.

——, T. R. Nathan, and J. L. Stanford, 1988: Barotropic stability of realistic stratospheric jets. *J. Atmos. Sci.*, **45**, 2545–2555.

Mechoso, C. R., D. L. Hartmann, and J. D. Farrara, 1985: Climatology and interannual variability of wave, mean-flow interaction in the Southern Hemisphere. *J. Atmos. Sci.*, **42**, 2189–2206.

Prata, A. J., 1984: The 4-day wave. *J. Atmos. Sci.*, **41**, 150–155.

Randel, W. J., 1987: The evaluation of winds from geopotential height data in the stratosphere. *J. Atmos. Sci.*, **44**, 3097–3120.

Salby, M. L., 1982: Sampling theory for asymptotic satellite observations. Part II: Fast Fourier synoptic mapping. *J. Atmos. Sci.*, **39**, 2602–2614.

Schoeberl, M. R., and R. S. Lindzen, 1984: A numerical simulation of barotropic instability. Part I: Wave–mean flow interaction. *J. Atmos. Sci.*, **41**, 1368–1379.

Smith, W. L., H. M. Woolf, C. M. Hayden, D. Q. Wark, and L. M. McMillin, 1979: The TIROS-N Operational Vertical Sounder. *Bull. Amer. Meteor. Soc.*, **58**, 1177–1187.

Venne, D. E., and J. L. Stanford, 1979: Observation of a 4-day temperature wave in the polar winter stratosphere. *J. Atmos. Sci.*, **36**, 2016–2019.

——, and ——, 1982: An observational study of high-latitude planetary waves in winter. *J. Atmos. Sci.*, **39**, 1026–1034.